Control System of the Array Antenna Test Bed

W. Gawronski[1] and H. Cooper[1]

The array antenna test bed is a scaled model of the array antenna, designed and built to test antenna control system hardware, to test the development of control software, and to verify the control system algorithms. This article presents the development of the test-bed control system model of an array antenna and the analysis of its performance. It starts with the models of the mechanical hardware, which are combined into the rate-loop model and finally into the position-loop model. The control system algorithms consist of the command preprocessor, the position controller, the rate controller, and the backlash controller. The simulation results of the rate-loop model and the position-loop model show close coincidence with the test data. The analysis showed that the test-bed rate-loop bandwidth is 70 Hz and the position-loop bandwidth is 16 Hz, which exceed the expected system performance requirements.

I. Introduction

This article describes the components of the control system of the array antenna test bed and their analytical models. The component models are combined into the test-bed control system, which includes the rate loop and the position loop. The performances of the rate and position loops of the test bed were obtained from the analysis of the servo model and the test results.

The test bed is shown in Fig. 1. It consists of an optical telescope mounted on a platform that rotates with respect to the horizontal (or elevation) axis and a turntable that rotates with respect to the vertical (or azimuth) axis. The rotations with respect to the elevation (EL) axis are actuated with the jackscrew and a motor, and the rotations with respect to the azimuth (AZ) axis are actuated with two motors, two reducers, and a bull gear (see Fig. 2). The drive motors are DC brushless motors supplied with the amplifiers and controllers. The telescope rotations are sensed with the azimuth and elevation encoders. The test bed is used to examine the usefulness of the control system of the future 12-m array antennas in terms of performance and cost.

The test-bed drives are different from the beam-waveguide (BWG) antenna drives. The differences are given in Table 1. As the table shows, the test-bed controller is fully digital—i.e., it consists of digital rate and position loops as well as a digital backlash control. Digital controllers are low maintenance and highly versatile. The test-bed motors are brushless and low maintenance. The linear quadratic Gaussian (LQG) algorithm is proposed for the rate loop, which increases precision pointing in wind gusts; see [1].
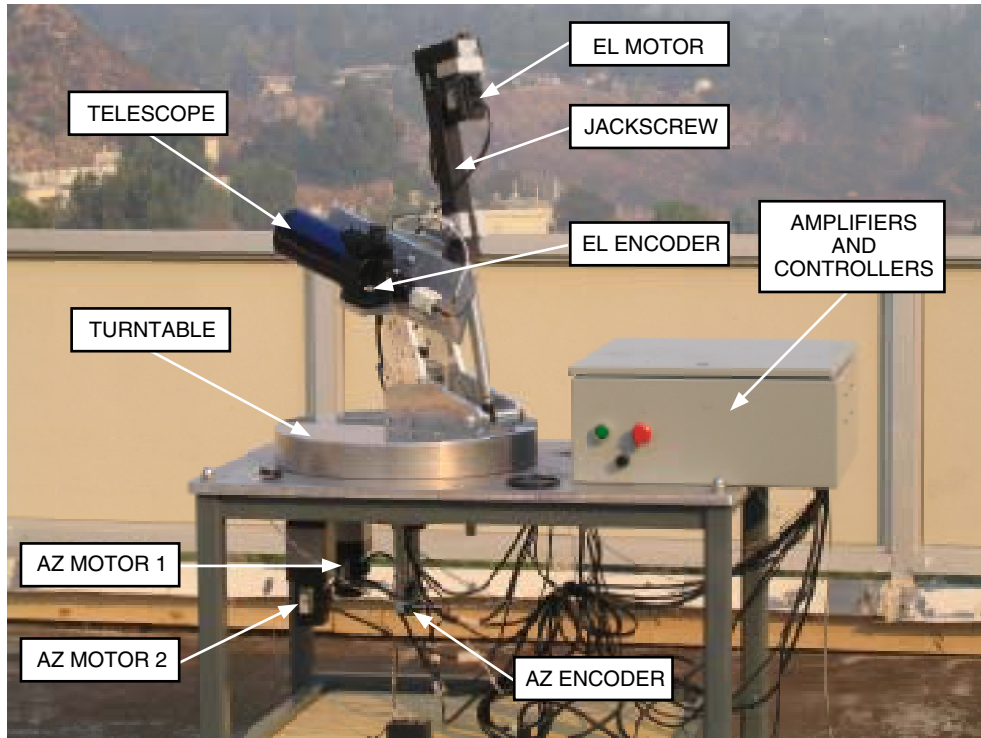

Fig. 1. The array antenna test bed.

Fig. 2. Test-bed bull gear with two pinions.

Table 1. BWG versus test-bed drives.

BWG antenna	Test bed
DC brush motors	DC brushless motors
Analog rate loop	Digital rate loop
Analog backlash control	Digital backlash control
Proportional rate loop	LQG rate loop
LQG position loop	LQG position loop

II. Test-Bed Model

For the sake of brevity, we describe the azimuth drive only. The elevation drive performance is very similar to that of the azimuth drive, as presented below.

The Simulink model of the test bed (azimuth axis) is shown in Fig. 3. In terms of hardware, it consists of a motor, amplifier, controller, reducer with drive shaft, and inertia dish. In terms of control function, it consists of the rate-loop model, rate and acceleration limiters, position controller with feedforward loop, command preprocessor, and backlash compensation algorithm. The control components are described in the following subsections. The test-bed data are given in Table 2.

A. The Rate-Loop Model

The rate-loop model is shown in Fig. 4. The sampling time is $\Delta t = 0.005$ s. It consists of a rigid gearbox with ratio $N_g = 280$; rotor dynamics; a motor armature; current feedback gain, k_{ip}; rate-feedback gain, k_{rp}; and torque bias.

1. The Motor Armature Model. In this model, the motor position, θ_m, is controlled by the armature voltage, u_a:

$$u_a = L_a \frac{di_a}{dt} + R_a i_a + k_b \dot{\theta}_m \tag{1}$$

where R_a is motor resistance, L_a is motor inductance, and k_b is the armature constant. The Simulink model representing the above equation is shown in Fig. 5. The motor torque, T_m, is proportional to the motor current, i_a:

$$T_m = k_t i_a \tag{2}$$

where k_t is the motor-torque constant.

2. The Model of Rotor Dynamics. In this model, the motor torque, T_m, is in equilibrium with the inertia and damping torque acting on the rigid rotor. Therefore,

$$T_m = J_m \ddot{\theta}_m + d_m \dot{\theta}_m \tag{3}$$

and J_m is total inertia of the motor. The Simulink discrete-time model representing Eq. (3) is shown in Fig. 6.

3. The Rate Controller. The rate controller is an LQG type of controller, although for the test-bed purposes only its proportional part was used. The proportional gain is $k_{\text{rate}} = 1.2$.
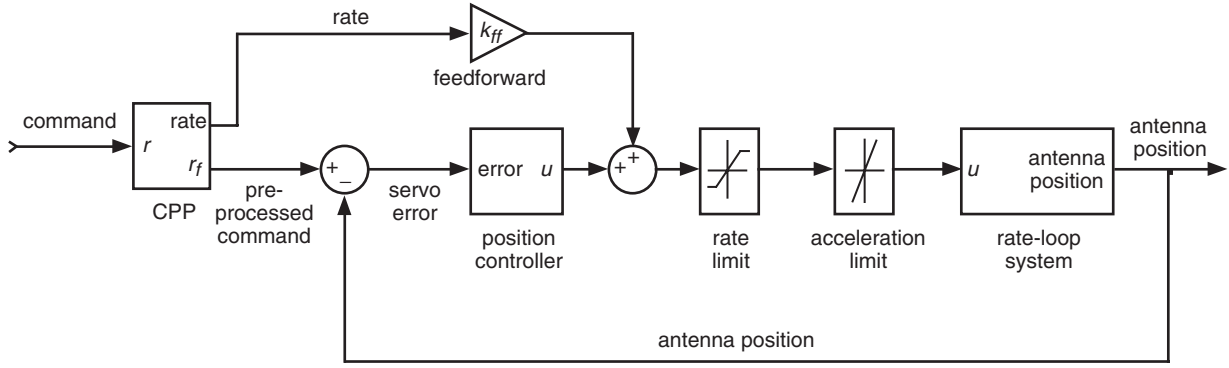
Fig. 3. Test-bed model.

Table 2. Test-bed data (motor GMBM60100-29).

| Parameter value	Parameter name
$R_a = 2.5\,\Omega$	Motor resistance
$L_a = 0.00737$ H	Motor inductance
$J_m = 1.14 \times 10^{-5}$ kg m^2	Motor inertia
$d_m = 4.52 \times 10^{-6}$ Nm s/rad	Motor damping, Eq. (3)
$N_g = 280$	Reducer gear ratio
$k_t = 0.206$ Nm/A	Motor-torque constant, Eq. (2)
$k_{\text{rate}} = 1.2$	Rate-loop gain
$k_p = 8.0$	Proportional gain
$k_i = 8.0$	Integral gain
$v_{\max} = 1.4$ deg/s	Rate limit
$a_{\max} = 1.4$ deg/s^2	Acceleration limit
$e_{i\,\max} = 0.5$ deg s	Limit of the integral error
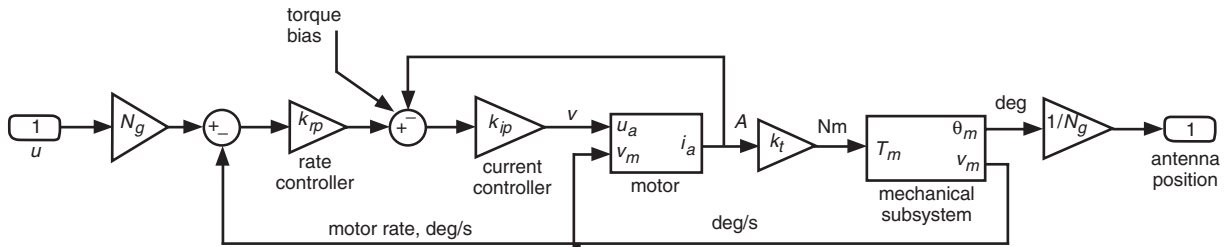
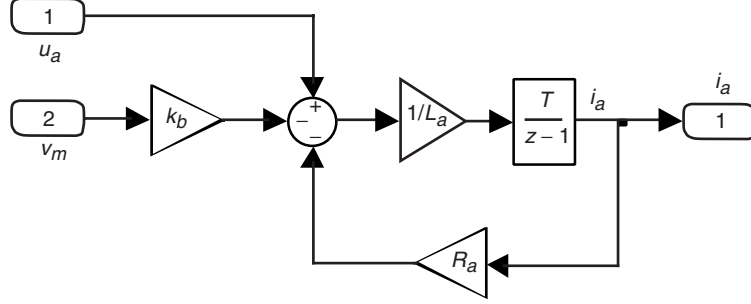**Fig. 4. Rate-loop system model.**
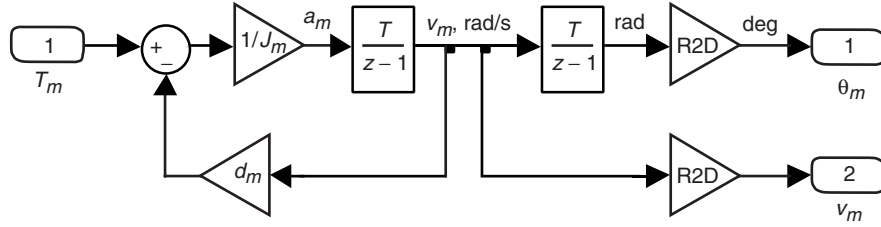
Fig. 5. Motor model; see Eq. (1).

Fig. 6. Mechanical subsystem model; see Eq. (3). (R2D = 180/π.)

B. Rate and Acceleration Limits

A rate limit of 1.4 deg/s and an acceleration limit of 1.4 deg/s^2 are imposed.

C. Position Controller

The position controller is an LQG type of controller, although for the test-bed purposes only its proportional-and-integral (PI) part was used. The position controller also includes a feedforward loop. The PI-part model is shown in Fig. 7. The integral is saturated at the value of integral error, $e_i = 0.5$ deg/s. The PI controller gains are as follows: the proportional gain is $k_p = 8.0$, and the integral gain is $k_i = 8.0$.

The feedforward part is shown in Fig. 3, and its rate gain is $k_{ff} = 1$. It feeds the command rate directly to the drives, improving the test-bed tracking performance.

D. Command Preprocessor

We implement a command preprocessor (CPP) because of the imposed rate and acceleration limits. Typically, the limits are violated during slewing, when large position offsets are applied as slewing commands. When limits are exceeded, the antenna dynamics are no longer linear, and the antenna becomes unstable, which is observed in the form of limit cycling (a periodical motion of constant magnitude and low frequency). One can avoid the instability by properly shaping the commands such that the limits are not violated.

The command preprocessor is a software unit that leaves the test-bed commands unaltered if they do not exceed the rate and/or acceleration limits and modifies the commands to the maximum acceleration and rate limits if the limits are exceeded. The block diagram of the CPP model is shown in Fig. 8.

The presented CPP algorithm differs from the one implemented at the BWG antennas, as presented in [2]. The BWG type of CPP cannot be implemented at the test bed due to the limitations of the
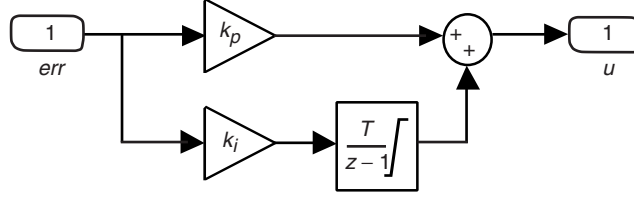
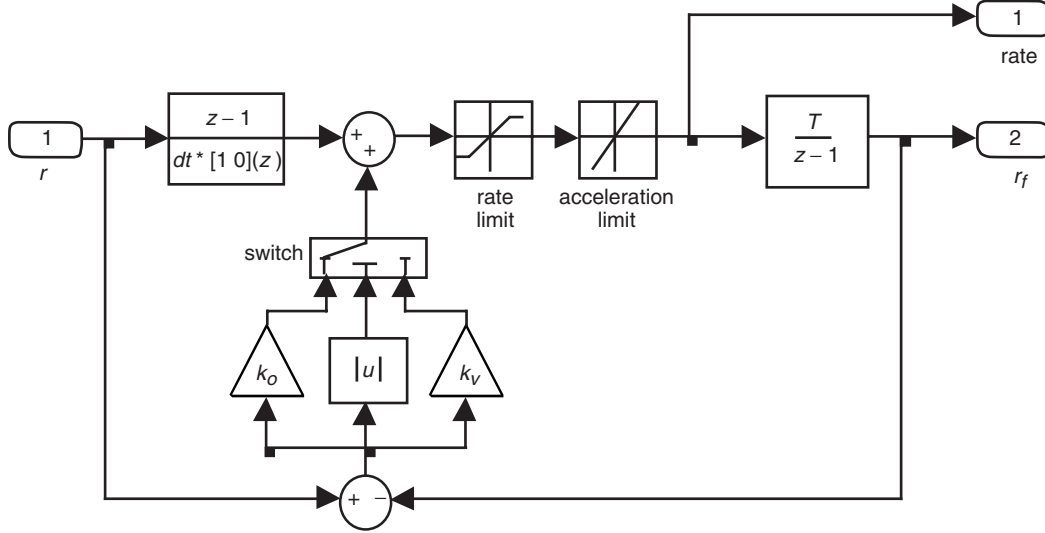**Fig. 7. Position controller model.**

Fig. 8. CPP model.

Pascal programming language used for the test-bed drive control. Pascal does not allow one to calculate accurately the exponential function required for a BWG type of CPP. For this reason, the test-bed CPP is modified such that its gain, k_{cpp}, switches from its lower value, k_o, to its upper value, k_v, rather than varying exponentially. The switching occurs at the selected value of the CPP error. The CPP error, e, is defined as the difference between the CPP input, r, and output, r_f, i.e., $e = r - r_f$. Thus, the CPP gain is defined as

$$k_{cpp} = \begin{cases} k_o & \text{for } |e| \geq e_o \\ k_v & \text{for } |e| < e_o \end{cases} \quad (4)$$

where $e_o = 0.01$ deg is the error threshold, while $k_o = 1.0$, and $k_v = 5.0$.

E. Backlash Compensation

The backlash that appears at the reducers' gears is controlled by adding an additional torque, ΔT, to the first azimuth drive and subtracting the same amount of torque from the second drive; see Figs. 9(a) and 4. The torque difference, ΔT, is called countertorque. The countertorque generated between the drives eliminates the backlash. We chose this difference to be $2\Delta T = 0.05 T_{\max}$, where $T_{\max}$ is the maximal allowable torque. It can be increased up to $0.15 T_{\max}$ if necessary.

More complex backlash compensation is shown in Fig. 9(b), where the countertorque, ΔT, depends on the antenna load; see Fig. 10. It is chosen such that, for a large load, $\Delta T = 0$. Also, a low-pass filter is added in order to suppress high-frequency dynamics in the backlash loop. The fast-varying load should
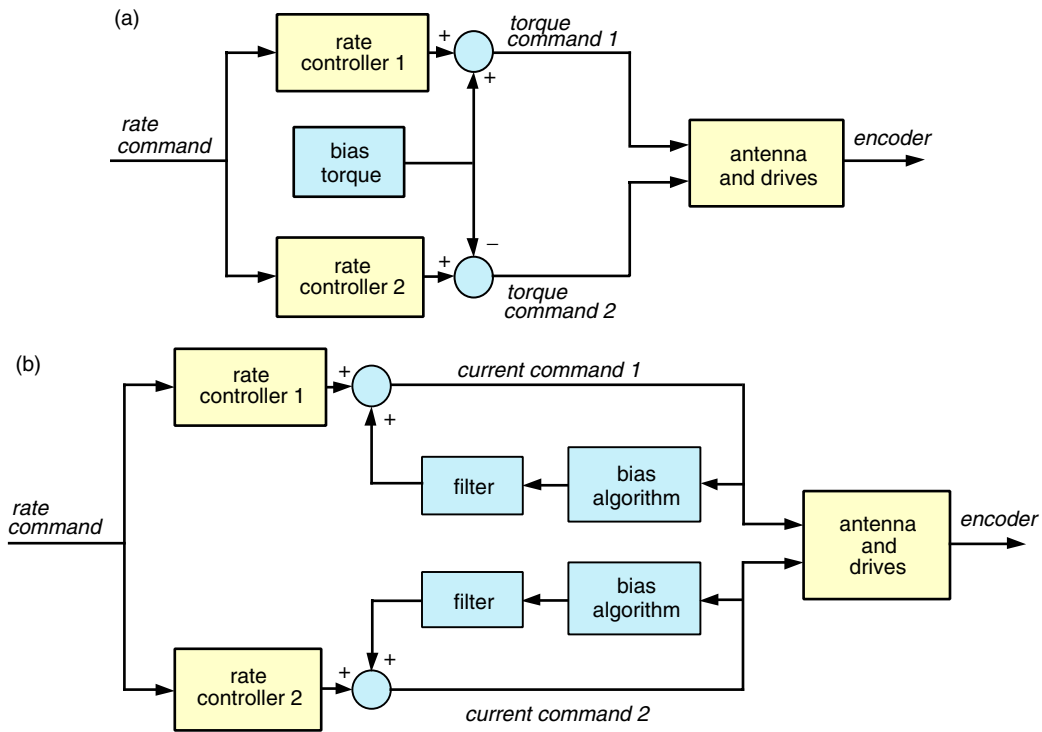
Fig. 9. Backlash compensation scheme: (a) with constant bias torque and (b) with bias torque dependent on the antenna load.
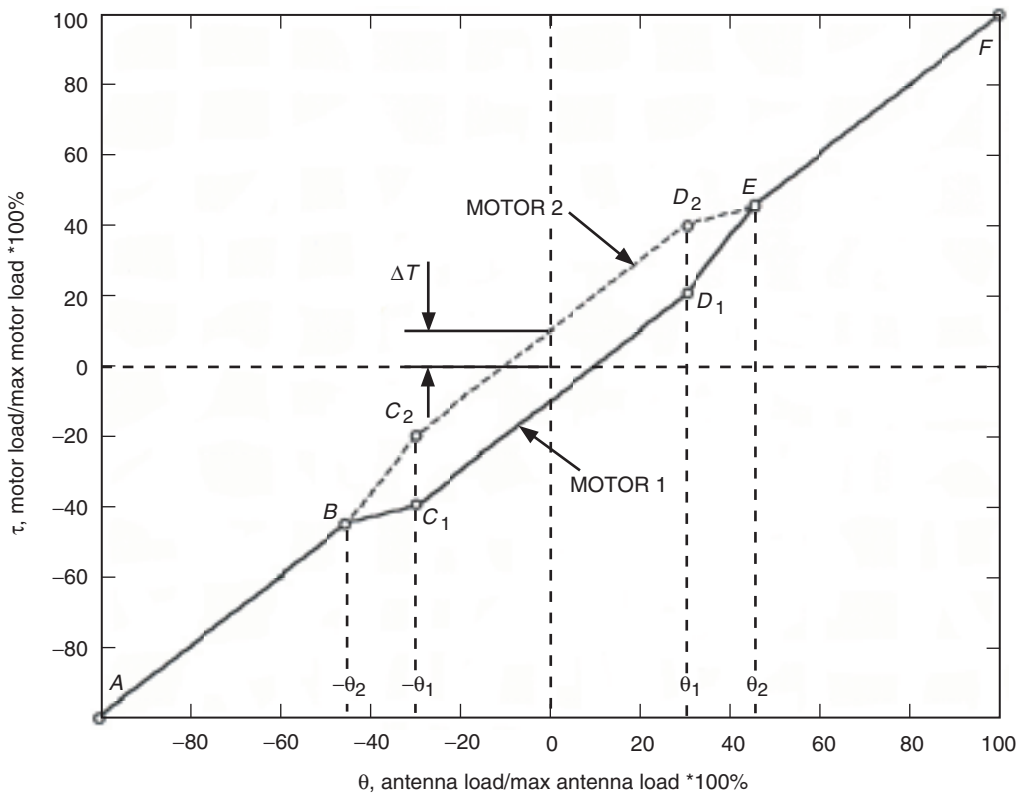

Fig. 10. Motor 1 and motor 2 loads versus antenna total load.

have little influence on the countertorque value. The filter bandwidth is 1 Hz. Its transfer function is as follows:

$$F(s) = \frac{1}{s+1} \tag{5}$$

For the sampling time $\Delta t = 0.005$ s, we have the discrete-time form of the above transfer function:

$$F(z) = \frac{0.00498752}{z - 0.9950125} \tag{6}$$

which translates into the following time-domain algorithm:

$$u_{fi+1} = 0.9950125 u_{fi} + 0.00498752 u_i \tag{7}$$

where u_i is the input to the filter at time $i\Delta t$ and u_{fi} is the output of the filter at time $i\Delta t$.

The backlash algorithm, as shown in Fig. 10, is as follows. Denote

$$\delta = \frac{\Delta \tau}{\theta_2 - \theta_1} \tag{8}$$

Then the equations for motor 1 are

$$\tau = \begin{cases} \theta & \text{for } \theta \in [-100, -\theta_2] & (\text{segment } AB) \\ (1-\delta)\theta - \delta\theta_2 & \text{for } \theta \in [-\theta_2, \theta_1] & (\text{segment } BC_1) \\ \theta - \Delta\tau & \text{for } \theta \in [-\theta_1, \theta_1] & (\text{segment } C_1 D_1) \\ (1+\delta)\theta - \delta\theta_2 & \text{for } \theta \in [\theta_1, \theta_2] & (\text{segment } D_1 E) \\ \theta & \text{for } \theta \in [\theta_2, 100] & (\text{segment } EF) \end{cases} \tag{9}$$

Equations for motor 2 are as follows:

$$\tau = \begin{cases} \theta & \text{for } \theta \in [-100, -\theta_2] & (\text{segment } AB) \\ (1+\delta)\theta + \delta\theta_2 & \text{for } \theta \in [-\theta_2, -\theta_1] & (\text{segment } BC_2) \\ \theta + \Delta\tau & \text{for } \theta \in [-\theta_1, \theta_1] & (\text{segment } C_2 D_2) \\ (1+\delta)\theta + \delta\theta_2 & \text{for } \theta \in [\theta_1, \theta_2] & (\text{segment } D_2 E) \\ \theta & \text{for } \theta \in [\theta_2, 100] & (\text{segment } EF) \end{cases} \tag{10}$$

III. Rate-Loop Performance

The rate-loop performance is evaluated through its bandwidth. Based on the Deep Space Network antenna data, the required rate-loop bandwidth is 50 Hz or higher. The rate-loop transfer function is shown in Fig. 11. The plots show that the rate-loop bandwidth is 70 Hz, which satisfies the requirement.

IV. Position-Loop Performance

The position-loop performance is evaluated by its bandwidth, settling time in step responses, and steady-state servo error in the rate offsets. The expected bandwidth is 10 Hz or higher; the settling time is 2 s or less; and the steady-state error in rate offsets is zero.

The transfer function of the position-loop model (from the test-bed position command to the encoder) is shown in Fig. 12 and was obtained from the Simulink model shown in Fig. 4. The plots show that the position-loop bandwidth is 16 Hz for the controller with the feedforward loop and 1.6 Hz for the controller without the feedforward loop. Thus, the test bed with the feedforward loop satisfies the bandwidth requirement.

The step responses—obtained from the Simulink model and from the test data—are shown in Fig. 13. Figure 13(a) presents the test-bed response to a small step of 0.02 deg. The settling time is 0.7 s, which exceeds the requirements. It shows quite good coincidence of the simulation and test data, except for the overshoot of 0.0025 deg, which is the value of the encoder resolution and could be the result of dry friction. Note the stepping plot of the test data, which is the result of low resolution of the encoder. The large step responses (of 10 deg), shown in Fig. 13(b), are smooth due to CPP action. They show good coincidence of test and simulation data.

The servo errors of the rate-offset responses are shown in Fig. 14. There is a considerable discrepancy between the simulation and test results. The transient servo errors obtained from tests are significantly larger than the servo errors from simulations. The probable cause of this discrepancy is a substantial amount of friction in the test bed, which was not modeled in the Simulink model. Note, however, that in both cases the steady-state servo error is zero, as required.

The test-bed performance is presented in Table 3.

V. Conclusions

This article presents the array antenna servo system test bed—its analysis and test data. The analysis and test results coincide and show that the test bed satisfies the requirements.

References

[1] W. Gawronski and K. Souccar, "Control Systems of the Large Millimeter Telescope," *The Interplanetary Network Progress Report 42-154, April–June 2003*, Jet Propulsion Laboratory, Pasadena, California, pp. 1–17, August 15, 2003.
http://ipnpr.jpl.nasa.gov/tmo/progress_report/42-154/154D.pdf

[2] W. Gawronski, "Command Preprocessor for the Beam-Waveguide Antennas," *The Telecommunications and Mission Operations Progress Report 42-136, October–December 1998*, Jet Propulsion Laboratory, Pasadena, California, pp. 1–10, February 15, 1999.
http://tmo.jpl.nasa.gov/tmo/progress_report/42-136/136A.pdf
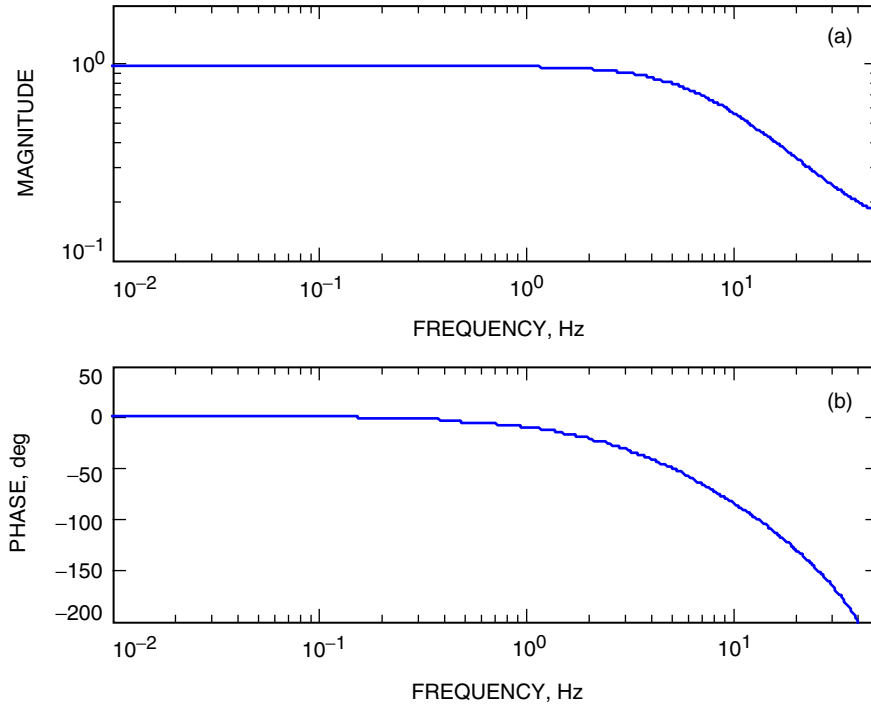
Fig. 11. The rate-loop transfer function: (a) magnitude and (b) phase. The rate-loop bandwidth is 70 Hz.
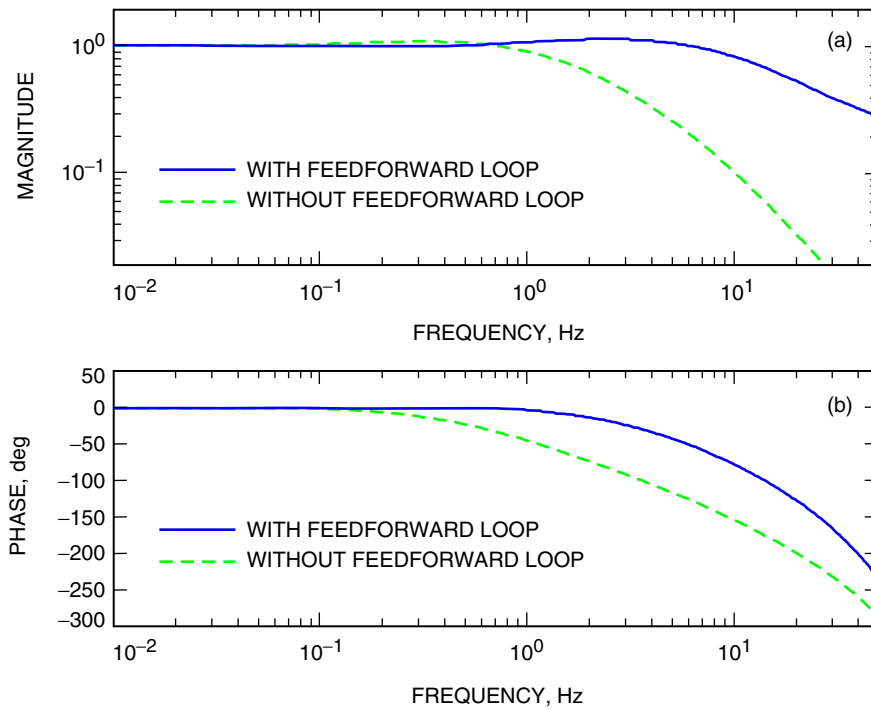

Fig. 12. Transfer functions of the test bed with and without the feedforward loop: (a) magnitude and (b) phase. The bandwidths of the test bed without and with the feedforward loop are 1.6 Hz and 16 Hz, respectively.
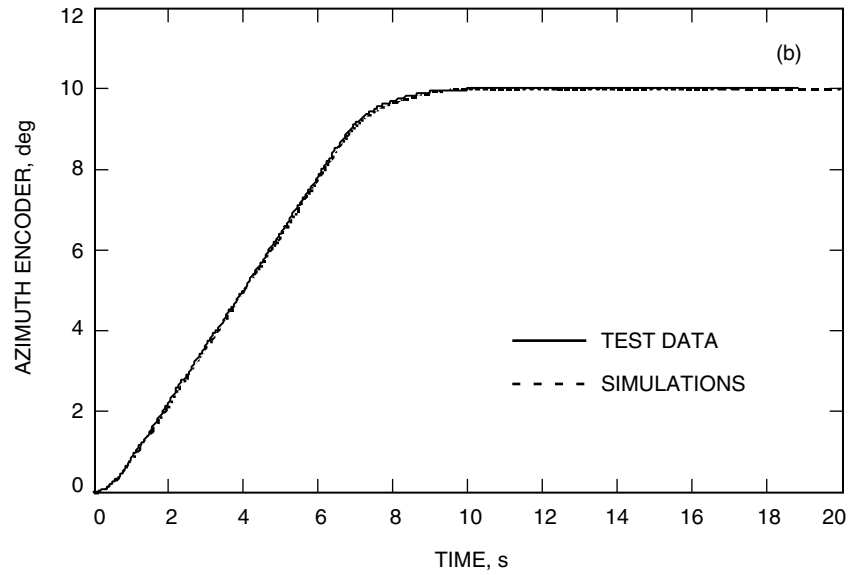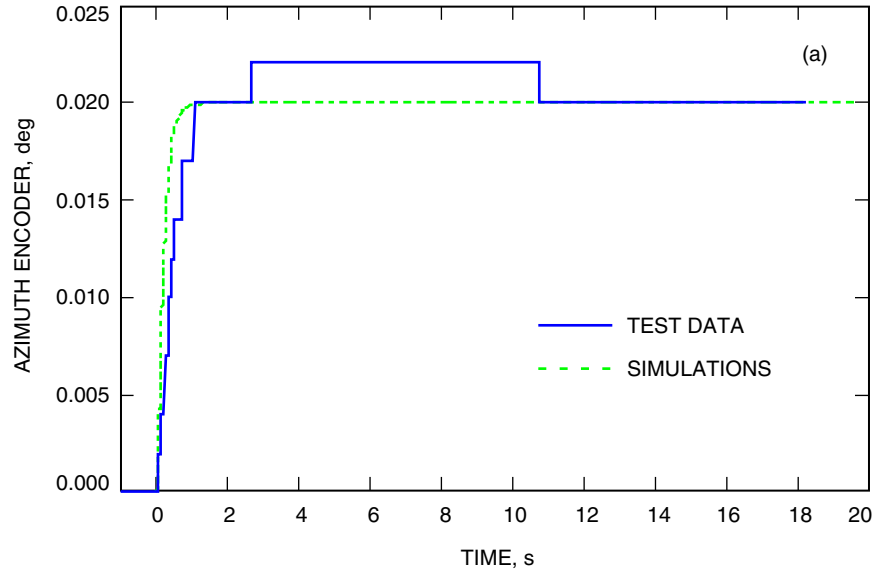
Fig. 13. Test-bed responses to (a) 20-mdeg step and (b) 10-deg step
(test data and simulation results overlap).

Table 3. Array antenna test-bed performance.

Rate-loop bandwidth, Hz	Position-loop bandwidth, Hz	Position-loop settling time, s	Position-loop steady-state error, mdeg
70	16	0.7	0
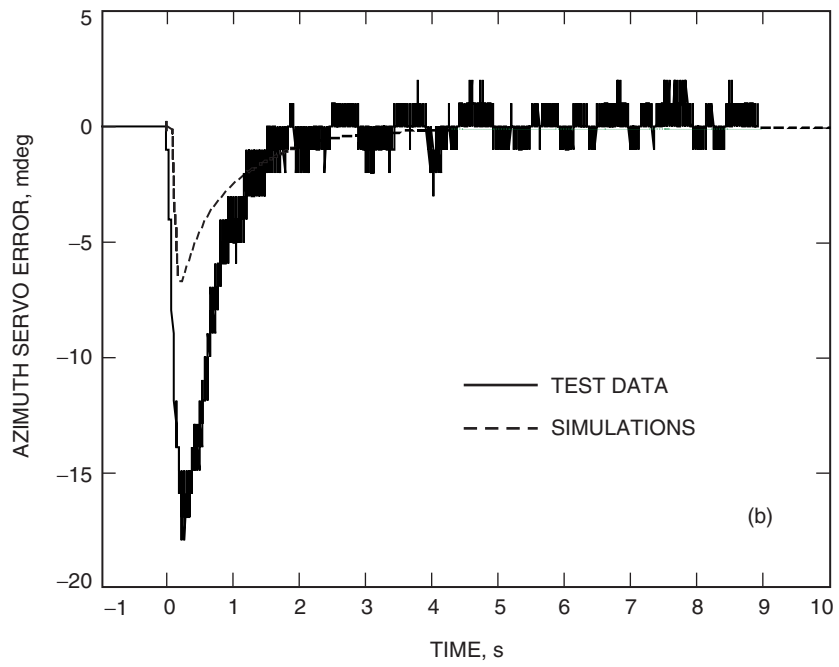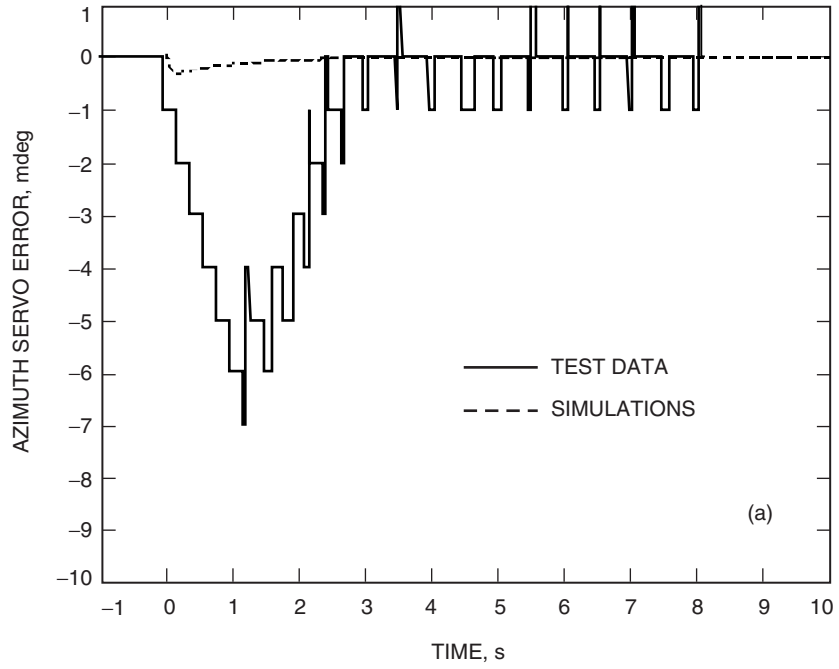
Fig. 14. Test-bed servo error for (a) 5-mdeg/s rate offset and
(b) 100-mdeg/s rate offset.